An Adaptive Nonlinear PID Design for 6-DOF Underwater Robotic Vehicle

Mustafa Wassef HASAN, Nizar Hadi ABBAS

Department of Electrical Engineering, College of Engineering, University of Baghdad, Karrada, 10001 Baghdad, Iraq

m.hasan0902@coeng.uobaghdad.edu.iq, dr.nizar.hadi@coeng.uobaghdad.edu.iq

DOI: 10.15598/aeee.v20i2.4370

Article history: Received Sep 27, 2021; Revised Dec 10, 2021; Accepted Jan 16, 2022; Published Jun 30, 2022.

Abstract. *An Adaptive Nonlinear PID (ANLPID) controller for six Degrees of Freedom (6-DOF) Underwater Robotic Vehicle (URV) model is proposed to solve the path tracking problem. The path tracking problem is mainly caused by external environmental disturbances and the unknown uncertainties of the URV model. The ANLPID controller is used to estimate both the external disturbances and the unknown URV uncertainties. The performance of the ANLPID controller was evaluated by comparing the ANLPID controller with other existing works that are Nonlinear PID (NLPID) controller and Nonlinear Fractional PID (NLFOPID) controller. The system stability is proved by utilizing the Lyapunov function. At the end, the results obtained show the proficiency of the ANLPID controller, where the ANLPID controller improved the performance of the URV by 41.4185 % compared to the NLPID controller and by 54.6479 % compared to the NLFOPID controller.*

Keywords

Adaptive Nonlinear PID (ANLPID), Nonlinear PID (NLPID), Nonlinear Fractional Order PID (NLFOPID), Underwater Robotic Vehicle (URV).

1. Introduction

The underwater robotic vehicle has received a lot of attraction in the recent years due to its several applications in various fields, such as the oil industry, military applications, communications, scientific research for the marine species, search and rescue, etc. The researchers provide several modeling and controlling techniques to solve or improve a specific issue. For e.g., the authors in [1] discuss the technical issue regarding the Autonomous Underwater Vehicle (AUV) in environmental monitoring of oil and gas industry risks. The authors in [2] present a new routing protocol for underwater wireless sensor networks. In [3], the authors proposed underwater acoustic networks to provide communication links between underwater vehicles. In [4], researchers study the Benthopelagic animals by using the Multibeam Echo Eounders (MBES) on the underwater vehicle. Finally, in [5], the author presents a mathematical model approach to reduce time and save more lives during search and rescue operations.

In recent years, different controllers have been proposed to solve several problems and issues that are faced by the unmanned robots, such as [6] where the authors propose an energy based variable structure controller approach for motion planning of unmanned robots or in [7] where the authors propose a fuzzy sliding mode controller for a mobile robot to eliminate the disturbances. In addition to that, the underwater robotic vehicle also play an important part in the development of controller designs, such as self-tuning PID [8] and [9], adaptive control [10], model reference adaptive PID [11], adaptive mutation genetic algorithm [12], adaptive low-level control [13], sliding mode controller [14] and [15], adaptive sliding mode controller [16], nonlinear fractional-order PID [17], H-infinity control [18].

The most known issue encountered by the URVs is the external disturbances and unknown uncertainties, which leads to path tracking problem. As a result of this, many researchers around the globe focus on this problem, such as [19] and [20] where the authors pro-

posed an adaptive neural network for trajectory tracking in the presence of external disturbances and uncertainties. However, such methods are sometimes limited to specific movements and are expensive. Thus, motivated by the last point, an Adaptive Nonlinear PID (ANLPID) controller is proposed to overcome this issue, where the feasibility of such design gives the URV the robustness required to estimate the disturbances and uncertainties and then eliminate these effects to reduce the error between the desired trajectory and the output trajectory. In real-time, this design gives the flexibility to overcome the side effects of the disturbances and uncertainties with a symbol and low-cost design.

The ANLPID shows good performance to eliminate the external disturbances and handle the uncertainty of the URV when compared to Nonlinear PID (NLPID) controller [21] and Nonlinear Fractional Order PID (NLFOPID) controller [17]. The performance of the URV with ANLPID, NLPID, and NLFOPID controllers is measured by taking an average of eight runnings for each controller, where each run represents a complete operation of the proposed controllers. The results show that the ANLPID improved the URV responses by 41.4185 % compared to the NLPID controller and by 54.6479 % compared to the NLFOPID controller.

The remainder of this work is structured as follows. Section 2. provides the details for the URV model designs. The Adaptive Nonlinear PID (ANLPID) controller design is stated in Sec. 3. Then, the fundamental result of this work and some numerical simulations to verify the efficiency of the presented controller are proposed in Sec. 4. At the end, the conclusion part is presented in Sec. 5.

2. URV Model Design

The URV model used in this work is based on [22] and [23], where the URV reference frames are described as either inertial or body reference frame (IRF and BRF), respectively. Some authors have defined the IRF as an Earth Reference Frame (ERF) [24]. Figure 1 demonstrates the URV reference frames. The ERF is defined as the vector $\eta = [x, y, z, \phi, \theta, \psi]^T$ where $\eta_1 = [\ x,\ y,\ z]^T$ explained as the position vector of the URV, while vector $\eta_2 = [\phi, \theta, \psi]^T$ illustrated as the rotational coordinates of the URV. The BRF refers to the URV degree of freedom, where it is defined as translational components (Surge, Sway, Heave) and rotational components (Roll, Pitch, Yaw). The linear and angular velocities of the URV are described by the vector $v = [\ u,\ v,\ w,\ p,\ q,\ r]^T$, where the vector $v_1 = [\ u,\ v,\ w]^T$ defined as the linear velocity of

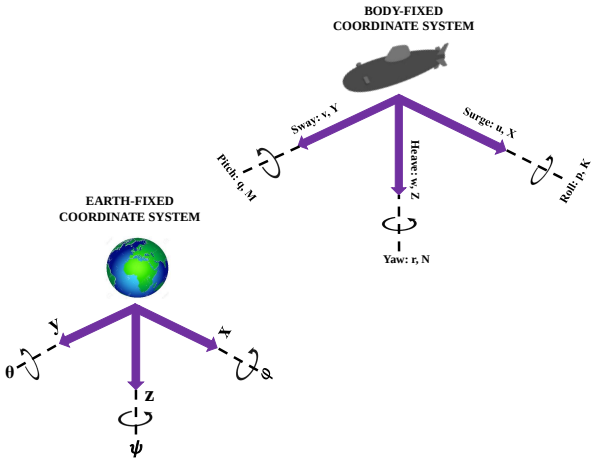

Fig. 1: URV reference frame.

the URV translational components, while the vector $v_2 = [\ p,\ q,\ r]^T$ defined as the angular velocities of the URV rotational components. The URV vehicle dynamics described by [25] as follows:

$$\mathbf{M}\dot{v} + \mathbf{C}(v)v + \mathbf{D}(v)v + \mathbf{g}(\eta) = F_\eta + \mathbf{D}(t), \quad (1)$$

where $\mathbf{M} \in R^{6\times6}$ is the inertia matrix, $\mathbf{C}(v) \in R^{6\times6}$ is the Coriolis and Centripetal matrix, $\mathbf{D}(v) \in R^{6\times6}$ defined as the hydrodynamic damping of the vehicle, $\mathbf{g}(\eta) \in R^6$ defined as the buoyancy and gravitational vector, $F_\eta \in R^6$ is the torque force applied on the URV and $\mathbf{D}(t) \in R^6$ is the disturbances developed on the system.

Now by transforming Eq. (1) into ERF, the following equation is presented:

$$\begin{aligned}\mathbf{M}_\eta(\eta)\ddot{\eta} + \mathbf{C}_\eta(v,\eta)\dot{\eta} + \mathbf{D}_\eta(v,\eta)\dot{\eta} + \mathbf{g}_\eta(\eta) = \\ = \mathbf{F}_\eta(\eta) + \mathbf{W}_\eta(t),\end{aligned} \quad (2)$$

where

$$\left\{\begin{array}{c}\left(\mathbf{M}_\eta\left(\eta\right) = J_{(\eta)}^{-T}\ \mathbf{M}\ J_{(\eta)}^{-1}\right), \\ \left(\mathbf{C}_\eta\left(\eta\right) = J_{(\eta)}^{-T}\left[\mathbf{C}\left(v\right) - \mathbf{M}\ J_{(\eta)}^{-1}\ \dot{J}_{(\eta)}\right]\ J_{(\eta)}^{-1}\right), \\ \left(\mathbf{D}_\eta\left(\eta\right) = J_{(\eta)}^{-T}\ \mathbf{D}\left(v\right)\ J_{(\eta)}^{-1}\right), \left(\mathbf{g}_\eta = J_{(\eta)}^{-T}\ \mathbf{g}_{(\eta)}\right), \\ \left(\mathbf{F}_\eta\left(\eta\right) = J_{(\eta)}^{-T}\ \mathbf{F}_\eta\right), \left(\mathbf{W}_\eta\left(t\right) = J_{(\eta)}^{-T}\ \mathbf{D}(t)\right),\end{array}\right\}$$

where $\mathbf{J}_\eta$ is the coordinate transformation matrix that relates the translational velocities between BRF and ERF.

The uncertainty used with this model can be expressed as [26]:

$$\mathbf{G}_s = \mathbf{B}_s^{-1}\mathbf{Q}_s + \mathbf{U}_i, \quad (3)$$

where $\dot{\mathbf{G}}_s = [\dot{u}, \dot{v}, \dot{w}, \dot{p}, \dot{q}, \dot{r}]^T$,
$\mathbf{Q}_s = \left[\sum X, \sum Y, \sum Z, \sum K, \sum M, \sum N\right]^T$ is the total

forces applied on the URV,
$\mathbf{U}_i = [U_u, U_v, U_w, U_p, U_q, U_r]^T$ is the lumped uncertainties that caused by internal noise caused by conductors or joints or by waves, $\mathbf{B}_s^{-1}$ represents the kinematic equation of the URV.

The disturbances developed on the URV model expressed as [26]:

$$\mathbf{D}(t) = \sum_{i=6}^{1} A_{1i}\cos(f_{1i}t) + A_{2i}\sin(f_{2i}t) + \text{randnoise}(0.1, 0.5), \quad (4)$$

where $(i = 1, 2, \ldots, 6)$, (A_{1i}, A_{2i}) defined as the amplitude of the waves,(f_{1i}, f_{2i}) represent the frequency of the waves in (radian), while the random noise is added to show the URV model's robustness with the proposed controllers.

Before going further with adaptive nonlinear PID controller design, the following assumptions are made:

Assumption 1. *By considering each of the surge, sway, and heave velocities are bounded, then* $\sup_{t\geq 0}|u| < K_u$, $\sup_{t\geq 0}|v| < K_v$, $\sup_{t\geq 0}|w| < K_w$, *where* K_u, K_v *and* K_w *parameters are defined as unknown constants.*

Remark 1. *Assumption (1) is always easy to verify [24]. Thus, it is considered limited.*

Assumption 2. *The desired path tracking trajectories are finite and bounded.*

Assumption 3. *The roll angle* ϕ*, pitch angle* θ*, and yaw angle* ψ *are less or equal to* π*.*

Remark 2. *According to [25] and [27], the URV in practice is not likely to reach* $|\theta| \leq \pi/2$ *because of the restoring force.*

Assumption 4. *The uncertainty values are considered to be bounded, such that* $|\mathbf{U}_i| \leq Y_i$, $(i = u, v, w, p, q, r)$, *while* Y_i *defined as unknown positive numbers.*

3. Adaptive Nonlinear PID Design

Most of the adaptive techniques lead to control saturation. Thus, Eq. (5) below is used to prevent control saturation caused by a large tracking error at the starting of the URV operation. Eq. (5) reduced the tracking error to a minimum as possible.

Thus, the primary nonlinear function used in the PID controller is expressed as:

$$\zeta_{e_i(t)} = \frac{N_{i1}\cdot\left(\dfrac{N_{i2}}{1+\exp(-2\cdot e_i(t))} - N_{i3}\right)}{N_{i4} + \left|\left(\dfrac{N_{i2}}{1+\exp(-2\cdot e_i(t))} - N_{i3}\right)\right|}, \quad (5)$$

where, the numerator term of Eq. (5) is defined as (tanh) function, and $e_i(t)$ is the error of the URV system and is expressed as:

$$e_i(t) = \eta_{id}(t) - \eta_i(t), \quad (6)$$

where $\eta_{id}(t)$ is the desired path tracking signal of the URV model, while $(N_{i1}, N_{i2}, N_{i3}$, and $N_{i4}) > 0$, and $i = 1, 2, \ldots, 6$.

Now, the final nonlinear function used in the PID controller is expressed as:

$$\xi_{e_i(t)} = \sigma_{i1} + \sigma_{i2}\cdot\tan^{-1}\left(\sigma_{i3}\cdot\exp\left(-\sigma_{i4}\cdot\zeta_{e_i(t)}\right)\right), \quad (7)$$

where σ_{i1}, σ_{i2}, σ_{i3}, and $\sigma_{i4} > 0$.

Figure 2 below show the nonlinear function used with PID controller at $N_{11} = 2$, $N_{12} = 2$, $N_{13} = 1$, $N_{14} = 2$, $\sigma_{11} = 1$, $\sigma_{12} = 1.274$, $\sigma_{13} = 0.5$, and $\sigma_{14} = 16$.

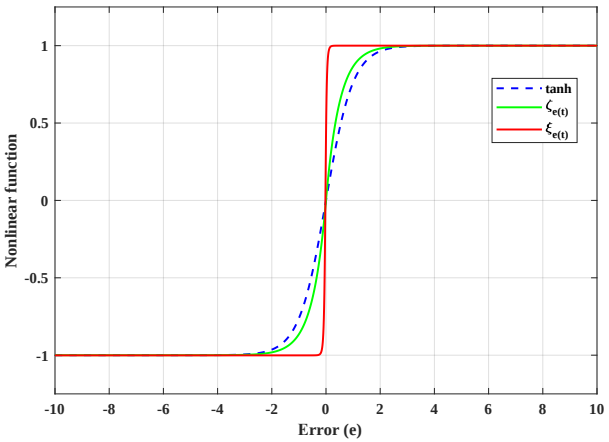

Fig. 2: Proposed nonlinear functions.

Theorem 1. *If assumptions (1), (2), (3), and (4) are satisfied [28] with the URV model in Eq. (2) and external disturbances in Eq. (4) and the uncertainty presented in Equation (3). Then, the URV model in Eq. (2) will be asymptotically stable. Thus, the URV model is described as follows:*

Denote $g_1 = \eta$, and $g_2 = \dot{\eta}$.

Next, we can write Eq. (2) as follows:

$$\begin{aligned}\dot{g}_1 &= g_2,\\ \dot{g}_2 &= -\mathbf{M}_{g_1}(g_1)^{-1}\left[\mathbf{C}_{g_1}(v, g_1)g_2 + \right.\\ &\quad \left. + \mathbf{D}_{g_1}(v, g_1)g_2 + \mathbf{g}_{g_1}(g_1) - \mathbf{F}_{g_1} - \mathbf{W}_{g_1}\right].\end{aligned} \quad (8)$$

Now, we can write Eq. (8) as follows:

$$\begin{aligned}\dot{g}_1 &= g_2,\\ \dot{g}_2 &= \boldsymbol{\delta}(g) + \mathbf{M}(g_1)\mathbf{F}_{g_1} + \mathbf{W}(t).\end{aligned} \quad (9)$$

where

$$\left\{\begin{array}{c}\boldsymbol{\delta}(g)=-\boldsymbol{M}_{g_1}(g_1)^{-1}\left[\mathbf{C}_{g_1}(v,g_1)g_2+\mathbf{D}_{g_1}(v,g_1)g_2\right.\\ \left.+\mathbf{g}_{g_1}(g_1)\right],\\ \mathbf{M}(g_1)=\mathbf{M}_{g_1}(g_1)^{-1}J(g_1)^{-1},\\ \mathbf{W}(t)=\mathbf{M}_{g_1}(g_1)^{-1}.\end{array}\right\}$$

Proof. Considering the URV mathematical model, the equation for the URV control law $\mathbf{F}_{g_1}$ is given by:

$$\mathbf{F}_{g_1}=\mathbf{M}(g_1)^{-1}\left[\ddot{\eta}_d-\hat{\boldsymbol{\delta}}(g)+\mathbf{K}^T\mathbf{X}-\hat{\mathbf{W}}(t)\right], \quad (10)$$

where $\hat{\boldsymbol{\delta}}(g)$ is the adaptive compensation and $\boldsymbol{K}^T=\left[K_p{}^*(t),\, K_i{}^*(t),\, K_d{}^*(t)\right]$, and $K_p{}^*(t)=K_p\cdot\xi_{e(t)}$, $K_i{}^*(t)=K_i\cdot\frac{d^{-1}\xi_{e(t)}}{dt^{-1}}$, $K_d{}^*(t)=K_d\cdot\frac{d\xi_{e(t)}}{dt}$, and $\mathbf{X}=\left[e,\varepsilon,\dot{e}\right]^T$
where

$$\varepsilon=\int_0^t e_i(\tau)d\tau. \quad (11)$$

Now, by substituting Eq. (10) into Eq. (9), we get the following equation:

$$\begin{array}{c}\dot{g}_2=\boldsymbol{\delta}(g)+\mathbf{M}(g_1)\mathbf{M}(g_1)^{-1}\left[\ddot{\eta}_d-\hat{\boldsymbol{\delta}}(g)+\right.\\ \left.+\mathbf{K}^T\mathbf{X}-\hat{\mathbf{W}}(t)\right]+\mathbf{W}(t).\end{array} \quad (12)$$

Simplifying Eq. (12) led to the following equation:

$$\ddot{\eta}=\boldsymbol{\delta}(g)+\ddot{\eta}_d-\hat{\boldsymbol{\delta}}(g)+\mathbf{K}^T\mathbf{X}+\mathbf{W}(t)-\hat{\mathbf{W}}(t)\xrightarrow{yields}$$

$$\ddot{\eta}-\ddot{\eta}_d=\boldsymbol{\delta}(g)-\hat{\boldsymbol{\delta}}(g)+\mathbf{K}^T\mathbf{X}+\boldsymbol{W}(t)-\hat{\mathbf{W}}(t)\xrightarrow{yields}$$

$$\ddot{e}=\hat{\boldsymbol{\delta}}(g)-\boldsymbol{\delta}(g)+\mathbf{K}^T\mathbf{X}+\mathbf{W}(t)-\mathbf{W}(t). \quad (13)$$

Then, Eq. (13) can be written as follows:

$$\begin{bmatrix}\dot{e}\\ \dot{\varepsilon}\\ \ddot{e}\end{bmatrix}=\begin{bmatrix}0 & 0 & 1\\ 0 & \frac{d}{dt} & 0\\ -K_p{}^*(t) & -K_i{}^*(t) & -K_d{}^*(t)\end{bmatrix}\begin{bmatrix}e\\ \varepsilon\\ \dot{e}\end{bmatrix}+$$
$$+\begin{bmatrix}0\\ 0\\ 1\end{bmatrix}\left[\hat{\boldsymbol{\delta}}(g)-\boldsymbol{\delta}(g)\right]+\begin{bmatrix}0\\ 0\\ 1\end{bmatrix}\left[\hat{\mathbf{W}}(t)-\mathbf{W}(t)\right]. \quad (14)$$

Next, Eq. (14) can be written as follows:

$$\dot{\mathbf{X}}=\beta\mathbf{X}+\mathbf{C}\left[\hat{\boldsymbol{\delta}}(g)-\boldsymbol{\delta}(g)\right]+\mathbf{A}\left[\hat{\mathbf{W}}(t)-\mathbf{W}(t)\right], \quad (15)$$

where $\beta=\begin{bmatrix}0 & 0 & 1\\ 0 & \frac{d}{dt} & 0\\ -K_p{}^*(t) & -K_i{}^*(t) & -K_d{}^*(t)\end{bmatrix}$ and $\mathbf{C}$, $\mathbf{A}=\begin{bmatrix}0 & 0 & 1\end{bmatrix}^T$.

Now, we assume the following candidate Lyapunov function to discuss the URV stability along with the proposed controller design:

$$V=V_1+V_2+V_3, \quad (16)$$

$$V=\frac{1}{2}\mathbf{X}^TP\mathbf{X}+\hat{\boldsymbol{\delta}}(g)+\hat{\mathbf{W}}(t)-\left(\int_0^e\gamma^TK_p{}^*(\gamma)\right.$$
$$\left.d(\gamma)+\int_0^e\gamma^TK_i{}^*(\gamma)d(\gamma)+\int_0^e\gamma^TK_d{}^*(\gamma)d(\gamma)\right), \quad (17)$$

where

$$V_1=\frac{1}{2}\mathbf{X}^TP\mathbf{X}. \quad (18)$$

Now, by differentiating Eq. (18), we get the following equation:

$$\dot{V}_1=\frac{1}{2}\left[\dot{\mathbf{X}}^TP\mathbf{X}+\mathbf{X}^TP\dot{\mathbf{X}}\right]. \quad (19)$$

Next, substitute Eq. (15) into Eq. (19), the following equation is obtained:

$$\begin{array}{c}\dot{V}_1=\frac{1}{2}\left[\beta^T\mathbf{X}^T+\mathbf{C}^T\hat{\boldsymbol{\delta}}(g)^T-\mathbf{C}^T\boldsymbol{\delta}(g)^T+\mathbf{A}^T\right.\\ \hat{\mathbf{W}}(t)^T-\mathbf{A}^T\mathbf{W}(t)^T\left]P\mathbf{X}+\frac{1}{2}\mathbf{X}^TP\right[\beta\mathbf{X}+\mathbf{C}^T\\ \left.\hat{\boldsymbol{\delta}}(g)-\mathbf{C}\boldsymbol{\delta}(g)+\mathbf{A}\hat{\mathbf{W}}(t)-\mathbf{A}\mathbf{W}(t)\right].\end{array} \quad (20)$$

Equation (20) is similar to the following equation:

$$\begin{array}{c}\dot{V}_1=\frac{1}{2}\left[\mathbf{X}^T\left[\beta^TP+\beta P\right]\mathbf{X}+\mathbf{X}P\mathbf{C}^T\hat{\boldsymbol{\delta}}(g)^T+\right.\\ +\mathbf{X}^TP\mathbf{C}\hat{\boldsymbol{\delta}}(g)-\mathbf{X}P\mathbf{C}^T\boldsymbol{\delta}(g)^T-\mathbf{X}^TP\mathbf{C}\boldsymbol{\delta}(g)+\\ +\mathbf{X}P\mathbf{A}^T\hat{\mathbf{W}}(t)^T+\mathbf{X}^TP\mathbf{A}\hat{\mathbf{W}}(t)+\\ \left.-\mathbf{X}P\mathbf{A}^T\mathbf{W}(t)^T-\mathbf{X}^TP\mathbf{A}\mathbf{W}(t)^T\right].\end{array} \quad (21)$$

where P is symmetric and positive definite matrix, which satisfies the following Lyapunov equation:

$$\beta^TP+\beta P=-Q,\, Q>0. \quad (22)$$

Now, by simplifying Eq. (21), we get the following equation:

$$\begin{array}{c}\dot{V}_1=-\frac{1}{2}\mathbf{X}^TQ\mathbf{X}+\mathbf{X}^TP\mathbf{C}\hat{\boldsymbol{\delta}}(g)-\mathbf{X}^TP\mathbf{C}\boldsymbol{\delta}(g)\\ +\mathbf{X}^TP\mathbf{A}\hat{\mathbf{W}}(t)-\mathbf{X}^TP\mathbf{A}\mathbf{W}(t).\end{array} \quad (23)$$

Then, the second part of the candidate Lyapunov function is given as follows:

$$V_2=\hat{\boldsymbol{\delta}}(g)+\hat{\mathbf{W}}(t). \quad (24)$$

Next, by differentiating Eq. (24), we get the following equation:

$$\dot{V}_2=\hat{\boldsymbol{\delta}}(g)\cdot\dot{\hat{\boldsymbol{\delta}}}(g)+\hat{\mathbf{W}}(t)\cdot\dot{\hat{\mathbf{W}}}(t). \quad (25)$$

Then, the third part of the candidate Lyapunov function is given as follows:

$$\begin{array}{c}V_3=\int_0^e\gamma^TK_p{}^*(\gamma)d(\gamma)+\int_0^e\gamma^TK_i{}^*(\gamma)d(\gamma)+\\ +\int_0^e\gamma^TK_d{}^*(\gamma)d(\gamma),\end{array} \quad (26)$$

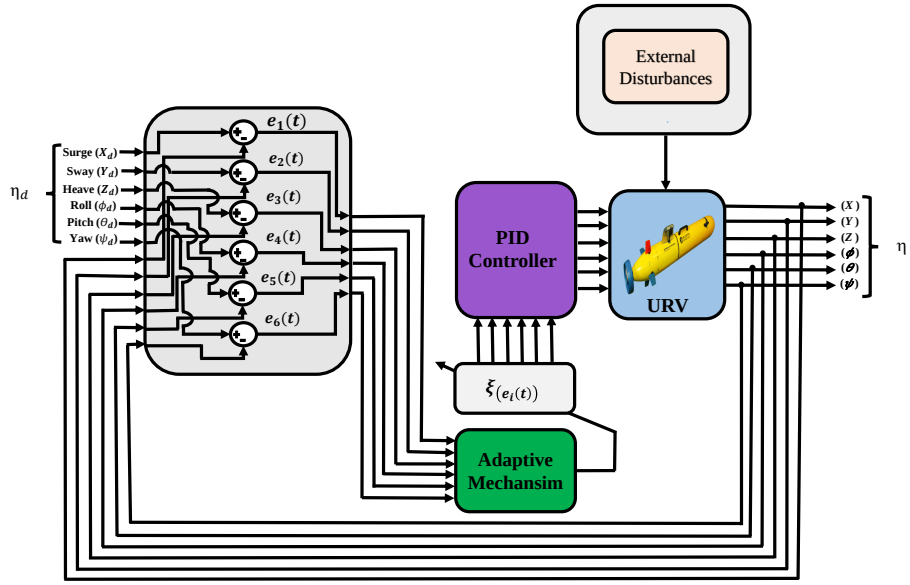

Fig. 3: ANLPID controller with URV model design.

where

$$\int_0^e \gamma^T K_p(\gamma) d(\gamma) = \int_0^{e_1} \gamma_1 K_{p1}(\gamma_1) d(\gamma_1) + \\ + \int_0^{e_2} \gamma_2 K_{p2}(\gamma_2) d(\gamma_2) + \int_0^{e_3} \gamma_1 K_{p3}(\gamma_3) d(\gamma_3) + \\ + \cdots + \int_0^{e_n} \gamma_n K_{pn}(\gamma_n) d(\gamma_n),$$

Then, according to Lemma 2 from [21] and [29], we can deduce that:

$$\int_0^e \gamma^T K_p(\gamma) d(\gamma) > 0 \; \forall \; e \neq \; 0 \in R^n, \tag{27}$$

and

$$\int_0^e \gamma^T K_p(\gamma) d(\gamma) \to \infty \; as \; ||e|| \to \infty. \tag{28}$$

Now, using the same arguments, we can conclude that the following conditions are accomplished:

$$\int_0^e \gamma^T K_i(\gamma) d(\gamma) \to \infty \; as \; ||e|| \to \infty, \tag{29}$$

$$\int_0^e \gamma^T K_i(\gamma) d(\gamma) \to \infty \; as \; ||e|| \to \infty, \tag{30}$$

and

$$\int_0^e \gamma^T K_d(\gamma) d(\gamma) \to \infty \; as \; ||e|| \to \infty, \tag{31}$$

$$\int_0^e \gamma^T K_d(\gamma) d(\gamma) \to \infty \; as \; ||e|| \to \infty. \tag{32}$$

Now, let the adaptive control law equal to the following equations:

$$\dot{\hat{\boldsymbol{\delta}}}(g) = \left[- \mathbf{X}^T P \mathbf{C} + \frac{\mathbf{X}^T P \mathbf{C}}{\hat{\boldsymbol{\delta}}(g)} \boldsymbol{\delta}(g) \right], \tag{33}$$

$$\dot{\hat{\mathbf{W}}}(t) = \left[- \mathbf{X}^T P \mathbf{A} + \frac{\mathbf{X}^T P \mathbf{A}}{\hat{\mathbf{W}}(t)} \mathbf{W}(t) \right]. \tag{34}$$

Next, we assume that the URV is moving at a low speed. Thus, we can conclude that $\mathbf{C}_\eta(v, \eta) = 0$. Then, by substituting Eq. (33) and Eq. (34) into Eq. (25), the overall time derivative of the Lyapunov function is defined as follows:

$$\dot{V} = -\frac{1}{2} \mathbf{X}^T Q \mathbf{X} - \dot{e}^T \mathbf{K}^T \dot{e}. \tag{35}$$

Finally, we can conclude that $\dot{V}$ is negative semi-definite and based on the LaSalle invariance principle, it is possible to ensure asymptotic stability. □

Figure 3 represent the ANLPID design with the URV model.

4. Results and Discussion

In this section, the URV model with the ANLPID controller performance is tested by monitoring the ANLPID controller across the URV path tracking trajectory on longitudinal and latitudinal areas. This URV trajectory is exposed to a particular disturbance area (three spots); each spot has different disturbance parameters to evaluate the ANLPID performance across different disturbances.

The ANLPID is compared with other controllers, such as, Nonlinear PID (NLPID) controller [21] and Nonlinear Fractional PID (NLFOPID) controller [17] to show their effectiveness. The collected results were simulated across a unique URV animation design. The

first procedure to obtain the results is to develop the URV model parameters given in [17].

The second step of the procedure is to identify the URV trajectory, where Eq. (36), Eq. (37), and Eq. (38) below represent the desired trajectory of the URV [30].

$$X_d = \begin{cases} 0.5\cos 0.5t & t < 4\pi, \\ 0.5 & t < 20, \\ 0.25t - 4.5 & t < 30, \\ 3 & otherwise, \end{cases} \tag{36}$$

$$Y_d = \begin{cases} 0.5\sin 0.5t & t < 4\pi, \\ 0.25 - \pi & t < 20, \\ 5 - \pi & t < 30, \\ -0.2358t - 8.94 & t < 40, \\ -0.5 & otherwise, \end{cases} \tag{37}$$

$$Z_d = \begin{cases} 0.125t + 1 & t < 4\pi, \\ 0.5\pi + 1 & t < 40, \\ \exp\left(-0.2 \cdot t + 8.944\right) & otherwise. \end{cases} \tag{38}$$

The roll angle is assumed to be ($\phi_d = \pi/11$), while the pitch angle is supposed to be ($\theta_d = \pi/6$). Finally, the desired yaw angle is supposed to be ($\psi_d = \pi/5$).

The URV trajectory is simulated across bathymetry data. The bathymetry data is used widely to describe the ocean and coasts graphs of the underwater vehicles and ships trajectories [31], [32] and [33]. Thus, we create bathymetry data using (Matlab R2018b) software, where the data is imported using GEBCO (General Bathymetric Chart of the Oceans) [34] and [35]. GEBCO is used to performed high-resolution data. The bathymetry data have the coordinate region ($west = 48°$, $east = 52°$, $south = 29°$, $north = 31°$).

At the end, the external disturbances locations are located, such that the first disturbance (D1) is located is at ($latitude(29°)$ and $longitude(50.5°)$). The second disturbance (D2) is located at ($latitude(29.6°)$ and $longitude(29.7°)$). In the end, the third disturbance (D3) is located at ($latitude(29.1°)$ and $longitude(48.7°)$). While the other disturbances (D4, D5, and D6) are used for each of the (roll, pitch, and yaw) angles, respectively. Figure 4 below represent the external disturbances developed on the URV model.

The results obtained from the ANLPID, NLPID, and NLFOPID controllers are shown in Fig. 5, such that the bathymetry data shows the URV path tracking trajectories for each of the developed controllers in addition to disturbance area locations which are represented as (red circles).

The results obtained show clearly that the ANLPID performs a nearly identical trajectory to the reference

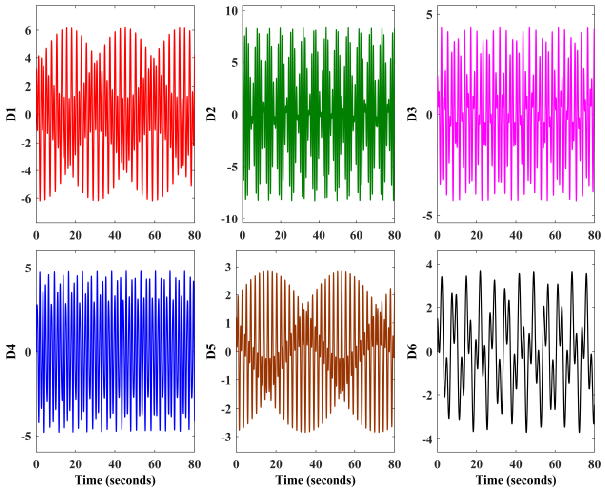

Fig. 4: External disturbances developed on the URV.

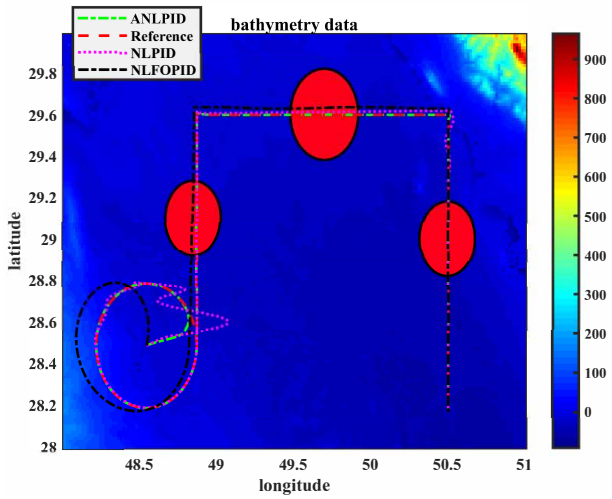

Fig. 5: The ANLPID, NLPID, and NLFOPID trajectories.

signal and acceptable performance to overcome the impact of the external disturbance as shown in Fig. 5 compared to the NLPID and NLFOPID controllers that show less performance than the ANLPID. Figure 5 combines the URV path tracking trajectories on the (X, Y, and Z) responses. Figure 6 represents the X, Y, Z, roll, pitch and yaw responses, respectively.

Next, we designed an animation model to create a moving URV model using Computer-Aided Design (CAD) [36] and [37]. The URV moves along a linear trajectory with external disturbances and uncertainties; Fig. 7 shows the (ANLPID, NLPID, and NLFOPID) performance with linear animation trajectory on disturbances area location (D1).

Figure 8 shows the (ANLPID, NLPID, and NLFOPID) performance with linear animation trajectory

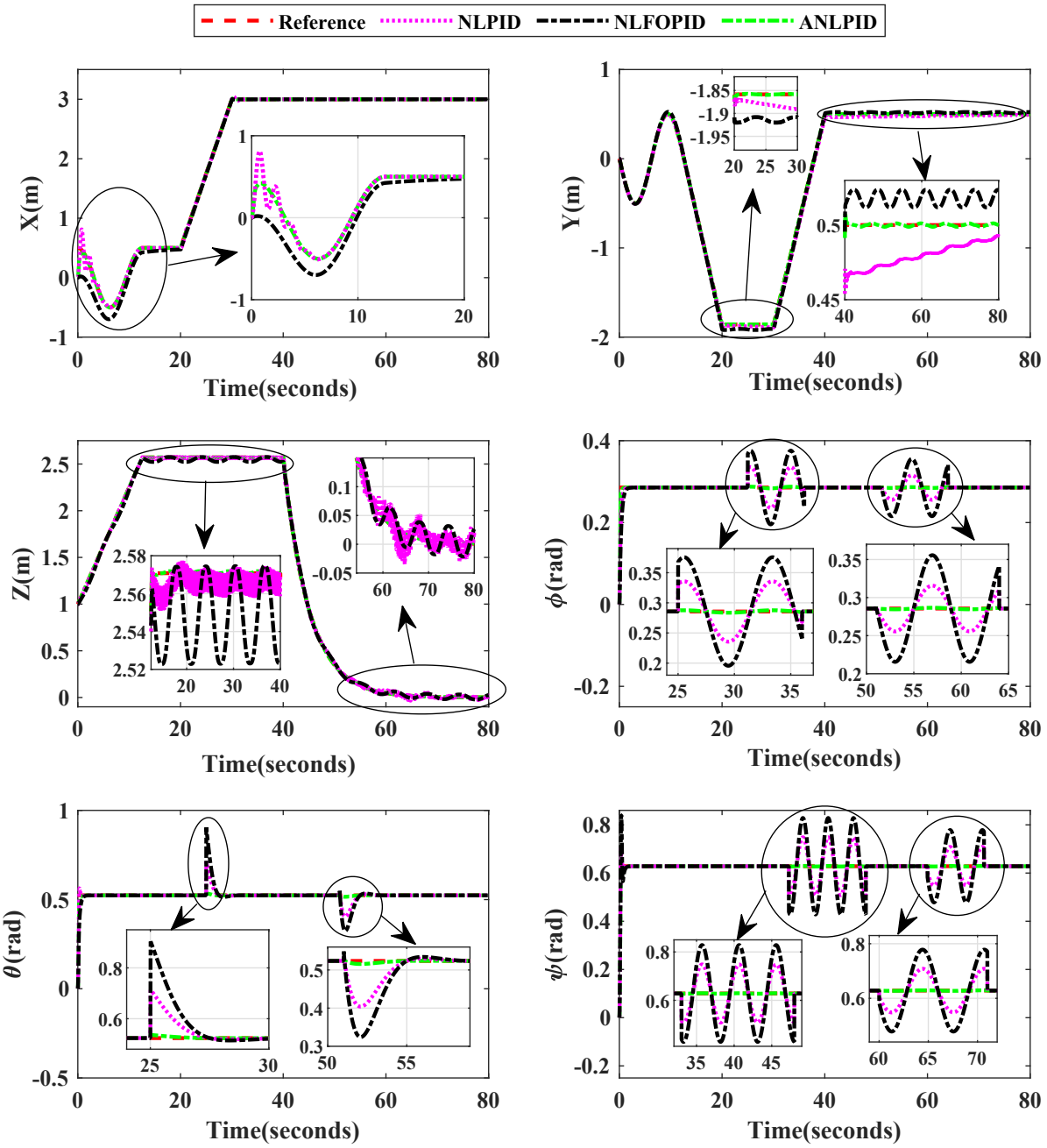

Fig. 6: Path following results of the developed controllers with URV model.

on disturbances area location (D2). Figure 9 shows the (ANLPID, NLPID, and NLFOPID) performance with linear animation trajectory on disturbances area location (D3).

To measure the performance of the URV with different controllers numerically, we proposed the following cost function:

$$Cost - Function_{ANLPID-NLPID-NLFOPID} = \\ = \int_0^t (\eta_d - \eta)^2 d\tau + \int_0^t |\eta_d - \eta| d\tau \quad (39)$$

where $ISE = \int_0^t (\eta_d - \eta)^2 d\tau$, and $IAE = \int_0^t |\eta_d - \eta| d\tau$.

The cost function used in this work depends on Integrated Square Error (ISE) and Integrated Absolute Error (IAE), where ISE is used to hold and reduce the cycle time of the URV response. At the same time, IAE was used to minimize the oscillation resulted from ISE [38] and [39]. Equation (39) show the total cost functions used in this work.

To measure the performance of the URV with different controllers, we used a numerical experiment, where an average of eight samples was calculated. Each sam-

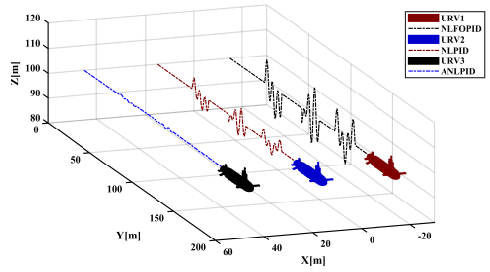

Fig. 7: Linear trajectory result for different developed controllers on (D1).

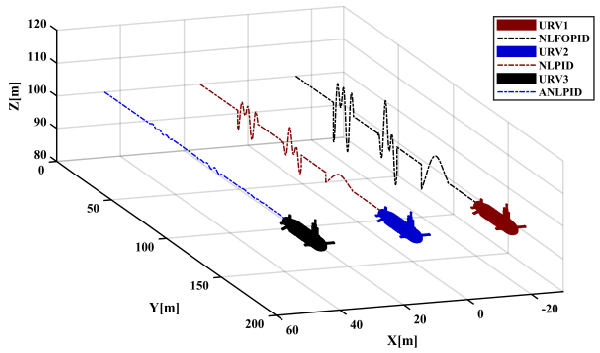

Fig. 8: Linear trajectory result for different developed controllers on (D2).

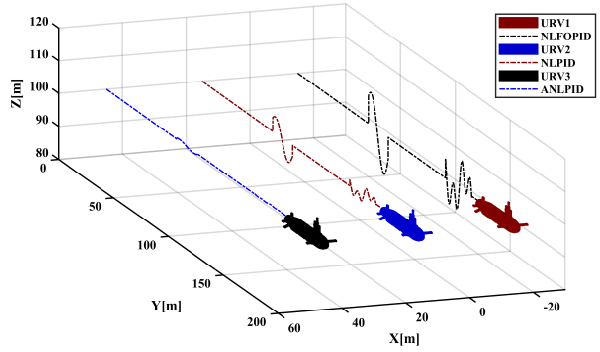

Fig. 9: Linear trajectory result for different developed controllers on (D3).

ple represents a full operation of the presented controllers (ANLPID, NLPID, and NLFOPID) with the URV model. Table 1 and Fig. 10 shows the calculated cost function samples of the proposed controllers. The following equation measures the total performance of the URV:

$$EP]_{\text{controller } A \text{ over controller } B} = \left(1 - \frac{CF]_A}{CF]_B}\right) \cdot 100\% \tag{40}$$

EP, is the enhancement percentage of different controllers used with URV and CF, refers to the cost functions of URV with a specific controller (ANLPID, NLPID, NLFOPID).

Tab. 1: Cost function samples of proposed controllers (ANLPID, NLPID, NLFOPID).

Sample	ANLPID	NLPID	NLFOPID
1	44.1004	75.2318	97.0031
2	44.5322	75.6752	96.8399
3	44.2041	75.3220	97.5011
4	43.6857	75.7201	98.1909
5	44.5309	75.5195	97.2230
6	44.3503	74.7295	97.7444
7	43.8113	76.1081	97.8665
8	44.3991	75.3212	97.3401
Average	**44.2017**	**75.4534**	**97.4636**

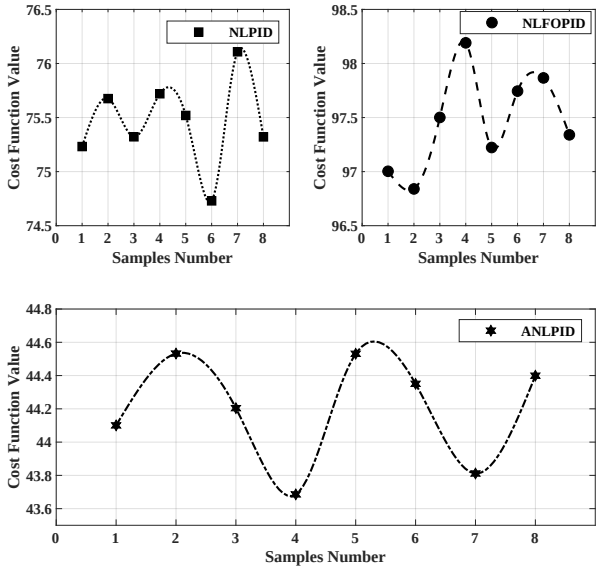

Fig. 10: Cost function samples representations.

The total average samples value of the ANLPID, NLPID and NLFOPID controllers was taken from Tab. 1 to represent the cost function parameters in Eq. (40).

The EP of the ANLPID controller compared to the NLPID controller can be calculated as follows:

$$EP]\frac{\text{ANLPID}}{\text{NLPID}} = \left(1 - \frac{44.2017}{75.4534}\right) \cdot 100\% = 41.4185\% \tag{41}$$

The EP of the ANLPID controller compared to the NLFOPID controller found as follows:

$$EP]\frac{\text{ANLPID}}{\text{NLFOPID}} = \left(1 - \frac{44.2017}{97.4636}\right) \cdot 100\% = 54.6479\% \tag{42}$$

5. Conclusion

A URV model is designed and simulated with an ANLPID controller to eliminate the unknown external environmental disturbances with the unknown uncertainty. The disturbances increased the overall nonlinearity of the URV, which led to the path tracking problem on the URV. The ANLPID compared with other controllers (NLPID and NLFOPID) to measure the performance of the URV and identified the best controller that performs the best path tracking. The results collected show that the ANLPID performs proficiently for the path tracking problem, where it improved the efficiency of the URV by 41.4185 % compared to the NLPID while it improved the URV efficiency by 54.6479 % compared to the NLFOPID. Future work would be to present other techniques with the ANLPID controller, such as neural and fuzzy techniques, to solve the accumulation of data in the underwater vehicle system for the IoT environment.

Author Contributions

M. W. H. designed the model, the software, visualization, and analysed the data in addition to writing. N. H. A. supervised the project and contributed to the design and implementation in addition to writing and editing.

References

[1] NIU, H., S. ADAMS, K. LEE, T. HUSAIN and N. BOSE. Applications of Autonomous Underwater Vehicles in Offshore Petroleum Industry Environmental Effects Monitoring. *Journal of Canadian Petroleum Technology*. 2009, vol. 48, iss. 5, pp. 12–16. ISSN 0021-9487. DOI: 10.2118/09-05-12-GE.

[2] FAROOQ, W., T. ALI, A. SHAF, U. DRAZ and S. YASIN. Atomic-shaped efficient delay and data gathering routing protocol for underwater wireless sensor networks. *Turkish Journal of Electrical Engineering & Computer Sciences*. 2019, vol. 27, iss. 5, pp. 3454–3469. ISSN 1303-6203. DOI: 10.3906/elk-1808-26.

[3] MARQUES, E. R. B., J. PINTO, S. KRAGELUND, P. S. DIAS, L. MADUREIRA, A. SOUSA, M. CORREIA, H. FERREIRA, R. GONCALVES, R. MARTINS, D. P. HONER, A. J. HEALEY, G. M. GONCALVES and J. B. SOUSA. AUV Control and Communication using Underwater Acoustic Networks. In: *OCEANS 2007 - Europe*. Aberdeen: IEEE, 2007, pp. 1–6. ISBN 978-1-4244-0634-0. DOI: 10.1109/oceanse.2007.4302469.

[4] DUNLOP, K. M., T. JARVIS, K. J. BENOIT-BIRD, C. M. WALUK, D. W.CARESS, H. THOMAS and K. L. SMITH. Detection and characterisation of deep-sea benthopelagic animals from an autonomous underwater vehicle with a multibeam echosounder: A proof of concept and description of data-processing methods. *Deep Sea Research Part I: Oceanographic Research Papers*. 2018, vol. 134, iss. 1, pp. 64–79. ISSN 0967-0637. DOI: 10.1016/j.dsr.2018.01.006.

[5] VENKATESAN, S. AUV for Search & Rescue at sea - an innovative approach. In: *2016 IEEE/OES Autonomous Underwater Vehicles (AUV)*. Tokyo: IEEE, 2016. pp. 1–9. ISBN 978-1-5090-2442-1. DOI: 10.1109/AUV.2016.7778711.

[6] BANIHANI, S., M. R. M. HAYAJNEH, A. AL-JARRAH and S. MUTAWE. New Control Approaches for Trajectory Tracking and Motion Planning of Unmanned Tracked Robot. *Advances in Electrical and Electronic Engineering*. 2021, vol. 19, iss. 1, pp. 42–56. ISSN 1804-3119. DOI: 10.15598/aeee.v19i1.4006.

[7] BENAZIZA, W., N. SLIMANE and A. MALLEM. Disturbances Elimination with Fuzzy Sliding Mode Control for Mobile Robot Trajectory Tracking. *Advances in Electrical and Electronic Engineering*. 2018, vol. 16, iss. 3, pp. 297–310. ISSN 1804-3119. DOI: 10.15598/aeee.v16i3.2767.

[8] DONG, E., S. GUO, X. LIN, X. LI and Y. WANG. A neural network-based self-tuning PID controller of an autonomous underwater vehicle. In: *IEEE International Conference on Mechatronics and Automation*. Chengdu: IEEE, 2012. pp. 898–903. ISBN 978-1-4673-1278-3. DOI: 10.1109/ICMA.2012.6283262.

[9] HERNANDEZ-ALVARADO, R., L. G. GARCIA-VALDOVINOS. T. SALGADO-JIMENEZ, A. GOMEZ-ESPINOSA and F. FONSECA-NAVARO. Neural Network-Based Self-Tuning PID Control for Underwater Vehicles. *Sensors*. 2016, vol. 16, iss. 9, pp. 1–18. ISSN 1424-8220. DOI: 10.3390/s16091429.

[10] YUH, J. and J. NIE. Application of non-regressor-based adaptive control to underwater robots: Experiment. *Computers & Electrical Engineering*. 2000, vol. 26, iss. 2, pp. 169–179. ISSN 0045-7906. DOI: 10.1016/S0045-7906(99)00039-7.

[11] SARHADI, P., A. R. NOEI and A. KHOSRAVI. Model reference adaptive PID control with anti-windup compensator for an autonomous under-

water vehicle. *Robotics and Autonomous Systems*. 2016, vol. 83, pp. 87–93. ISSN 0921-8890. DOI: 10.1016/j.robot.2016.05.016.

[12] DING, W., H. CAO, H. GUO, Y. MA and Z. MAO. Investigation on optimal path for submarine search by an unmanned underwater vehicle. *Computers & Electrical Engineering*. 2019, vol. 79, iss. 2019, pp. 1–11. ISSN 0045-7906. DOI: 10.1016/j.compeleceng.2019.106468.

[13] CARLUCHO, I., M. D. PAULA, S. WANG, Y. PETILLOT and G. G. ACOSTA. Adaptive low-level control of autonomous underwater vehicles using deep reinforcement learning. *Robotics and Autonomous Systems*. 2018, vol. 107, pp. 71–86. ISSN 0921-8890. DOI: 10.1016/j.robot.2018.05.016.

[14] JOE, H., M. KIM and S.-C. YU. Second-order sliding-mode controller for autonomous underwater vehicle in the presence of unknown disturbances. *Nonlinear Dynamics*. 2014, vol. 78, iss. 1, pp. 183–196. ISSN 1573-269X. DOI: 10.1007/s11071-014-1431-0.

[15] KIM, D., H.-S. CHOI, J.-Y. KIM, J.-H. PARK and N.-H. TRAN. Trajectory generation and sliding-mode controller design of an underwater vehicle-manipulator system with redundancy. *International Journal of Precision Engineering and Manufacturing*. 2015, vol. 16, iss. 7, pp. 1561–1570. ISSN 2005-4602. DOI: 10.1007/s12541-015-0206-y.

[16] GUO, Y., H. QIN, B. XU, Y. HAN, Q.-Y. FAN and P. ZHANG. Composite learning adaptive sliding mode control for AUV target tracking. *Neurocomputing*. 2019, vol. 351, iss. 1, pp. 180–186. ISSN 1872-8286. DOI: 10.1016/j.neucom.2019.03.033.

[17] HASAN, M. W and N. H. ABBAS. An improved swarm intelligence algorithms-based nonlinear fractional order-PID controller for a trajectory tracking of underwater vehicles. *Telkomnika*. 2020, vol. 18, iss. 6, pp. 3173–3183. ISSN 2302-9293. DOI: 10.12928/telkomnika.v18i6.16282.

[18] CHENG, X.-Q., J.-Y. QU, Z. P. YAN and X. Q. BIAN. H_∞ robust fault-tolerant controller design for an autonomous underwater vehicle's navigation control system. *Journal of Marine science and Application*. 2010, vol. 9, iss. 1, pp. 87–92. ISSN 1671-9433. DOI: 10.1007/s11804-010-8052-x.

[19] LI, J., J. DU and C. L. P. CHEN. Command-Filtered Robust Adaptive NN Control With the Prescribed Performance for the 3-D Trajectory Tracking of Underactuated AUVs. *IEEE Transactions on Neural Networks and Learning Systems*. 2021, vol. 1, iss. 1, pp. 1–13. ISSN 2162-2388. DOI: 10.1109/TNNLS.2021.3082407.

[20] ZHANG, J., X. XIANG, Q. ZHANG and W. LI. Neural network-based adaptive trajectory tracking control of underactuated AUVs with unknown asymmetrical actuator saturation and unknown dynamics. *Ocean Engineering*. 2020, vol. 218, iss. 1, pp. 1–12. ISSN 0029-8018. DOI: 10.1016/j.oceaneng.2020.108193.

[21] GUERRERO, J., J. TORRES, V. CREUZE, A. CHEMORI and E. CAMPOS. Saturation based nonlinear PID control for underwater vehicles: Design, stability analysis and experiments. *Mechatronics*. 2019, vol. 61, pp. 96–105. ISSN 0957-4158. DOI: 10.1016/j.mechatronics.2019.06.006.

[22] YANG, R., B. CLEMENT, A. MANSOUR, M. LI and N. WU. Modeling of a Complex-Shaped Underwater Vehicle for Robust Control Scheme. *Journal of Intelligent & Robotic Systems*. 2015, vol. 80, iss. 3, pp. 491–506. ISSN 1573-0409. DOI: 10.1007/s10846-015-0186-2.

[23] HASAN, M. W and N. H. ABBAS. Controller design for underwater robotic vehicle based on improved whale optimization algorithm. *Bulletin of Electrical Engineering and Informatics*. 2021, vol. 10, iss. 2, pp. 609–618. ISSN 2302-9285. DOI: 10.11591/eei.v10i2.2288.

[24] HASAN, M. W and N. H. ABBAS. Disturbance Rejection for Underwater robotic vehicle based on adaptive fuzzy with nonlinear PID controller. *ISA Transactions*. 2022. ISSN 0019-0578. DOI: 10.1016/j.isatra.2022.03.020

[25] FOSSEN, T. I. *Marine Control Systems Guidance, Navigation, and Control of Ships, Rigs and Underwater Vehicles*. 1st ed. Trondheim: Marine Cybernetics, 2002. ISBN 978-8-2923-5600-5.

[26] ZHANG, Y., X. WANG, S. WANG and J. MIAO. DO-LPV-based robust 3D path following control of underactuated autonomous underwater vehicle with multiple uncertainties. *ISA transactions*. 2020, vol. 101, iss. 1, pp. 189–203. ISSN 0019-0578. DOI: 10.1016/j.isatra.2020.01.017.

[27] DO, K. D and J. PAN. *Control of Ships and Underwater Vehicles: Design for Underactuated and Nonlinear Marine Systems*. 1st ed. London: Springer, 2009. ISBN 978-1-84882-730-1.

[28] WANG, J., C. WANG, Y. WEI and C. YHANG. Bounded neural adaptive formation control of multiple underactuated AUVs under uncertain dynamics. *ISA Transactions*. 2020,

vol. 105, iss. 1 pp. 111–119. ISSN 0019-0578. DOI: 10.1016/j.isatra.2020.06.002.

[29] HAMMAD, M. M., A. K. ELSHENAWY and M. I. EL SINGABY. Trajectory following and stabilization control of fully actuated AUV using inverse kinematics and self-tuning fuzzy PID. *PlOS ONE*. 2017, vol. 12, iss. 7, pp. 1–35. ISSN 1932-6203. DOI: 10.1371/journal.pone.0179611.

[30] SANTOS, M. A and G. V. RAFFO. Path tracking Model Predictive Control of a Tilt-rotor UAV carrying a suspended load. In: *2016 IEEE 19th International Conference on Intelligent Transportation Systems (ITSC)*. Rio de Janeiro: IEEE, 2016, pp. 1458–1463. ISBN 978-1-5090-1889-5. DOI: 10.1109/ITSC.2016.7795749.

[31] MA, T., Y. LI, R. WANG, Z. CONG and Y. GONG. AUV robust bathymetric simultaneous localization and mapping. *Ocean Engineering*. 2018, vol. 166, iss. 1, pp. 336–349. ISSN 0029-8018. DOI: 10.1016/j.oceaneng.2018.08.029.

[32] FRANCA, R. P., A. T. SALTON, R. D. S CASTRO, B. N. GREEN and D. MARELLI. Trajectory Generation for Bathymetry based AUV Navigation and Localization. *IFAC-PapersOnLine*. 2015, vol. 48, iss. 16, pp. 95–100. ISSN 2405-8963. DOI: 10.1016/j.ifacol.2015.10.264.

[33] BUSH, L. A. M., L. BLACKMORE and B. C. WILLIAMS. AUV bathymetric mapping depth planning for bottom following splice linear programming algorithm. In: *OCEANS 2016 MTS/IEEE Monterey Conference*. Monterey: IEEE, 2016. pp. 1–8. ISBN 978-1-5090-1537-5. DOI: 10.1109/OCEANS.2016.7761306.

[34] WYNN, R. B., V. A. I. HUVENNE, T. P. L. BAS, B. J. MURTON, D. P. CONNELLY, B. J. BETT, H. A. RUHL, K. J. MORIS, J. PEAKALL, D. R. PARSONS, E. J. SUMNER, S. E. DARBY, R. M. DORRELL and J. E. HUNT. Autonomous Underwater Vehicles (AUVs): Their past, present and future contributions to the advancement of marine geoscience. *Marine Geology*. 2014, vol. 352, iss. 1 pp. 451–468. ISSN 0025-3227. DOI: 10.1016/j.margeo.2014.03.012.

[35] LIU, Y., Z. WU, D. ZHAO, J. ZHOU, J. SHANG, M. WANG, C. ZHU and X. LUO. Construction of High-Resolution Bathymetric Dataset for the Mariana Trench. *IEEE Access*. 2019, vol. 7, iss. 1, pp. 142441–142450. ISSN 2169-3536. DOI: 10.1109/ACCESS.2019.2944667.

[36] ARAS, M. S. M., K. LI ZHE, M. K. ARIPIN, T. P. CHAING, H. N. M. SHAH, A. KHAMIS, N. NURDIANA and M. Z. A. RASHID. Design analysis and modelling of autonomous underwater vehicle (AUV) using CAD. *NIScPR Online Periodicals Repository*. 2019, vol. 48, iss. 7, pp. 1081–1090. ISSN 0975-1033. DOI: handle/123456789/48858.

[37] EDGE, C., S. S. ENAN, M. FULTON, J. HONG, J. MO, K. BARTHELEMY, H. BASHAW, B. KALLEVIG, C. KNUTSON, K. ORPEN and J. SATTAR. Design and Experiments with LoCO AUV: A Low Cost Open-Source Autonomous Underwater Vehicle. In: *2020 IEEE/RSJ International Conference on Intelligent Robots and Systems (IROS)*. Las Vegas: IEEE, 2021, pp. 1761–1768. ISBN 978-1-7281-6212-6. DOI: 10.1109/IROS45743.2020.9341007.

[38] SAHIB, M. A. and B. S. AHMED. A new multiobjective performance criterion used in PID tuning optimization algorithms. *Journal of advanced research*. 2016, vol. 7, iss. 1, pp. 125–134. ISSN 2090-1232. DOI: 10.1016/j.jare.2015.03.004.

[39] ABBAS, N. H. Tuning of different controlling techniques for magnetic suspending system using an improved bat algorithm. *International Journal of Electrical and Computer Engineering*. 2020, vol. 10, iss. 3, pp. 2402–2415. ISSN 2722-2578. DOI: 10.11591/ijece.v10i3.pp2402-2415.

About Authors

Mustafa Wassef HASAN received the B.Sc. degree in Electrical Engineering from University of Baghdad, Iraq, in 2017. He received the M.Sc. degree in Electrical Engineering from University of Baghdad, Iraq, in 2020. He has been working on projects related to robotics, nonlinear control, optimization algorithms, Computer-Aided Design (CAD).

Nizar Hadi ABBAS received his B.Sc. degree in electrical engineering from University of Baghdad, Baghdad, Iraq in 2000, a M.Sc. degree in control and computer engineering in 2002 from University of Baghdad, and a Ph.D. degree in advanced control in 2011 from Osmania University, Hyderabad, India. He is currently a professor at Electrical Engineering Department, University of Baghdad, Iraq. His research interests include control theory, controllers design, fractional order systems, robot modeling & control and modern optimization techniques.